# Temporal phase-unwrapping of static surfaces with 2-sensitivity fringe-patterns

**Manuel Servin,*** **J. M. Padilla, Adonai Gonzalez and Guillermo Garnica**

*Centro de Investigaciones en Optica A. C., Loma del Bosque 115, 37150 Leon Guanajuato, Mexico*
*mservin@cio.mx

**Abstract:** Here we describe a 2-step temporal phase unwrapping formula that uses 2-sensitivity demodulated phases for measuring static surfaces. The first phase demodulation has at most 1-wavelength sensitivity and the second one is *G*-times (*G*>>1.0) more sensitive. Measuring static surfaces with 2-sensitivity fringe patterns is well known and recent published methods combine 2-sensitivities measurements mostly by triangulation. Two important applications for our 2-step unwrapping algorithm is profilometry and synthetic aperture radar (SAR) interferometry. In these two applications the object or surface being analyzed is static and highly discontinuous; so temporal unwrapping is the best strategy to follow. Phase-demodulation in profilometry and SAR interferometry is very similar because both share similar mathematical models.



**OCIS codes:** (120.0120) Instrumentation, measurement, and metrology; (120.6650) Surface measurements, figure; (100.2650) Fringe analysis.

## References and links

1. J. M. Huntley and H. Saldner, “Temporal phase-unwrapping algorithm for automated interferogram analysis,” Appl. Opt. **32**(17), 3047–3052 (1993).
2. G. Pedrini, I. Alexeenko, W. Osten, and H. J. Tiziani, “Temporal phase unwrapping of digital hologram sequences,” Appl. Opt. **42**(29), 5846–5854 (2003).
3. H. O. Saldner and J. M. Huntley, “Temporal phase unwrapping: application to surface profiling of discontinuous objects,” Appl. Opt. **36**(13), 2770–2775 (1997).
4. J. L. Li, H. J. Su, and X. Y. Su, “Two-frequency grating used in phase-measuring profilometry,” Appl. Opt. **36**(1), 277–280 (1997).
5. J. Li, L. G. Hassebrook, and C. Guan, “Optimized two-frequency phase-measuring-profilometry light-sensor temporal-noise sensitivity,” J. Opt. Soc. Am. A **20**(1), 106–115 (2003).
6. E. H. Kim, J. Hahn, H. Kim, and B. Lee, “Profilometry without phase unwrapping using multi-frequency and four-step phase-shift sinusoidal fringe projection,” Opt. Express **17**(10), 7818–7830 (2009).
7. K. Liu, Y. Wang, D. L. Lau, Q. Hao, and L. G. Hassebrook, “Dual-frequency pattern scheme for high-speed 3-D shape measurement,” Opt. Express **18**(5), 5229–5244 (2010).
8. Y. Fu, W. Wang, and H. Xiao, “Three-dimensional profile measurement based on modified temporal phase unwrapping algorithm,” Optik (Stuttg.) **124**(6), 557–560 (2013).
9. Y. Xu, S. Jia, X. Luo, J. Yang, and Y. Zhang, “Multi-frequency projected fringe profilometry for measuring objects with large depth discontinuities,” Opt. Commun. **288**, 27–30 (2013).
10. T. Liu, C. Zhou, Y. Liu, S. Si, and Z. Lei, “Deflectometry for phase retrieval using a composite fringe,” Opt. Applicata **94**, 451–461 (2014).
11. J. Long, J. Xi, M. Zhu, W. Cheng, R. Cheng, Z. Li, and Y. Shi, “Absolute phase map recovery of two fringe patterns with flexible selection of fringe wavelengths,” Appl. Opt. **53**(9), 1794–1801 (2014).
12. Y. Xu, S. Jia, Q. Bao, H. Chen, and J. Yang, “Recovery of absolute height from wrapped phase maps for fringe projection profilometry,” Opt. Express **22**(14), 16819–16828 (2014).
13. G. Krieger, I. Hajnsek, K. P. Papathanassiou, M. Younis, and A. Moreira, “Interferometric Synthetic Aperture Radar (SAR) Missions Employing Formation Flying,” Proc. IEEE **98**(5), 816–843 (2010).
14. M. Servin, J. A. Quiroga, and J. M. Padilla, *Fringe Pattern Analysis for Optical Metrology* (Wiley-Vch, 2014).
15. K. J. Gasvik, *Optical Metrology*, 3th ed. (John Wiley & Sons, 2002).

## 1. Introduction

Temporal phase unwrapping was introduced by Huntley and Saldner [1] and it is used to measure optical dynamic wavefronts where one may change the number of interferometry fringes when testing a solid sustaining a dynamic loading [1]. Temporal unwrapping has also

#234984 - $15.00 USD Received 24 Feb 2015; revised 24 May 2015; accepted 26 May 2015; published 8 Jun 2015

been used for measuring a dynamic sequence of holograms [2]. As the name implies the unwrapping is not made in the spatial domain but in the temporal domain over a single spatial pixel. Each spatial pixel in the dynamic fringe pattern is unwrapped independently from the others. This has the advantage that noisy pixels remain isolated and do not spread their noise to less noisy regions ruining the entire spatial unwrapping process. The main drawback of temporal unwrapping is that it needs many wrapped intermediate temporal phase-maps to keep within the limits imposed by the Nyquist temporal sampling rate [1].

Saldner and Huntley [3] also applied temporal phase unwrapping to profilometry of discontinuous three-dimensional (3D) objects. Saldner and Huntley [3] stated that the Nyquist temporal sampling limit, allow them at most 1-wavelength ($1\lambda$) sensitivity increase per temporal step. Therefore if one wishes to pass from $1\lambda$ to $7\lambda$ in phase-sensitivity one would need 7 intermediate temporal phase-maps. Here we are proposing to use only the two extremes wrapped phases to obtain the same result. The Nyquist sampling limit is overcome because the profiling surface is static during the whole temporal fringe-projection profilometry experiment. Another way of seeing this is by noting that the static 2D surface measured at different phase sensitivities always have the same Shannon information entropy. This is because the surface remains static; the relative probability of occurrence of any given point in this surface is the same independently of the measuring sensitivity scale. That is why the Nyquist sampling limit is not a fundamental limit in this case.

Since the publication of reference [3] multi-sensitivity profilometry of 3D discontinuous static objects has been an active research field [4–12]. Profilometry of highly discontinuous industrial objects is the rule rather than the exception and temporal unwrapping is the best choice for these applications. These researches [3–12] have demonstrated and applied several algorithms to unwrap by triangulation and other varied techniques wrapped phases with many wavelengths from less sensitive phase-maps.

Another important field of applications of phase unwrapping with variable sensitivity interferometry is Synthetic Aperture Radar (SAR) Interferometry [13]. SAR interferometry is a powerful remote sensing technique for the quantitative measurement geophysical data of the Earth's surface. By increasing the baseline of the 2 Radar antennas, SAR interferometry enables sub-wavelength phase-measurements of the earth surface with variable sensitivity. Here also we can combine 2-sensitive SAR fringe-patterns to unwrap the highly discontinuous Earth terrain with the accuracy of the highest-baseline phase-measurement. Although 3D fringe projection profilometry and SAR interferometry need widely different experimental set-ups (SAR interferometry normally uses earth-orbiting satellites) both share the same formal or mathematical background.

Here we propose a 2-step temporal phase unwrapping algorithm which uses 2 widely separated sensitive demodulated-wrapped phases of a static surface.

## 2. Temporal phase unwrapping with sensitivity interferometric measurements

We start by giving the standard mathematical formula for two fringe patterns having different phase modulation sensitivity,

$$\begin{aligned} I1(x,y) &= a(x,y) + b(x,y)\cos\left[\varphi(x,y)\right], \quad \varphi(x,y) \in (-\pi,\pi), \\ I2(x,y) &= a(x,y) + b(x,y)\cos\left[G\,\varphi(x,y)\right], \quad (G \gg 1)\,,\, G \in \mathbb{R}. \end{aligned} \tag{1}$$

Here we are assuming that $\varphi(x,y)$ is a $1\lambda$ sensitive phase and $G\,\varphi(x,y)$ is $G$-times more sensitive, *i.e.* $\sup|G\,\varphi(x,y)| = G\lambda, (G \in \mathbb{R})$. One may use a large number of phase demodulation algorithms [14] to obtain the 2 demodulated wrapped phase-maps as,

$$\begin{aligned} \varphi 1(x,y) &= W\left[\varphi(x,y)\right], \qquad \varphi(x,y) \in (-\pi,\pi). \\ \varphi 2_W(x,y) &= W\left[G\varphi(x,y)\right], \qquad (G \gg 1)\,,\, G \in \mathbb{R}. \end{aligned} \tag{2}$$

#234984 - $15.00 USD Received 24 Feb 2015; revised 24 May 2015; accepted 26 May 2015; published 8 Jun 2015

Being $\varphi_W = W[\varphi] = \text{angle}[\exp(i\,\varphi)]$ the wrapping phase operator. Equation (2) shows the two demodulated phases of the 2 fringe-patterns in Eq. (1). The first demodulation $\varphi 1(x,y)$ is not wrapped because it is less than $1\lambda$; the second phase $\varphi 2_W(x,y)$ is highly wrapped because it is scaled-up by $G$ which in practice falls within $6 < G < 20$ $(G \in \mathbb{R})$ depending on the quality of $\varphi 1(x,y)$ and $\varphi 2_W(x,y)$.

### 3. Signal-to-noise ratio gain in 2-sensitivity phase modulation of static surfaces

From the phase-noise perspective there is a good advantage of using variable sensitivity interferometry. Let us assume that the two interferogram are phase modulated by $[\varphi(x,y) + \varphi n(x,y)]$ and by $[G\varphi(x,y) + \varphi n(x,y)]$ as,

$$\begin{aligned} I1(x,y) &= a(x,y) + b(x,y)\cos\left[\varphi(x,y) \quad + \varphi n(x,y)\right], \quad \varphi(x,y) \in (-\pi,\pi), \\ I2(x,y) &= a(x,y) + b(x,y)\cos\left[G\varphi(x,y) + \varphi n(x,y)\right], \; (G \gg 1)\,, G \in \mathbb{R}. \end{aligned} \tag{3}$$

Being $\varphi n(x,y)$ the phase-noise. The phase-noise is the same in both fringe-patterns because the experimental set-up is the same except for an increase $(G \gg 1)$ in phase-sensitivity. In an abstract Hilbert space, the power of a signal $s(x,y)$ is given by $\int \left|s(x,y)\right|^2 dxdy$; therefore the signal-to-noise power ratios for the modulating phases in Eq. (3) are,

$$\frac{\textit{Phase Signal Power}}{\textit{Phase Noise Power}} = \frac{\iint\limits_{(x,y)\in\Omega} \left|G\varphi(x,y)\right|^2 dxdy}{\iint\limits_{(x,y)\in\Omega} \left|\varphi n(x,y)\right|^2 dxdy} > \frac{\iint\limits_{(x,y)\in\Omega} \left|\varphi(x,y)\right|^2 dxdy}{\iint\limits_{(x,y)\in\Omega} \left|\varphi n(x,y)\right|^2 dxdy}. \tag{4}$$

Being $(x,y) \in \Omega$ the 2-dimensional region where the signal $\varphi(x,y)$ is well-defined. The signal-to-noise power-ratio increases $G^2$ times by increasing the phase sensitivity from $\varphi(x,y)$ to $G\varphi(x,y)$ for the same phase-noise $\varphi n(x,y)$. This is the fundamental reason why it is a good idea to use temporal phase unwrapping in digital 3D profilometry and in SAR interferometry of static surfaces. If we want to have $\varphi(x,y)$ as noiseless as $G\varphi(x,y)$ one would need $N$ $(N = G^2)$ phase-shifted fringe-patterns $I1(x,y)$ to obtain the same signal-to-noise than demodulating $I2(x,y)$ alone [14]

### 4. Temporal phase unwrapping of static surfaces with 2-measuring sensitivities

No matter which digital phase demodulation method one uses [14] the last step is always phase unwrapping. We are assuming that we end up with 2 wrapped phase measurements as,

$$\varphi 1(x,y) = W[\varphi(x,y)], \qquad \textit{and} \qquad \varphi 2_W(x,y) = W[G\varphi(x,y)], \quad (G \gg 1)\,, G \in \mathbb{R}. \tag{5}$$

Being $W[\varphi] = \text{angle}[\exp(i\,\varphi)]$ the wrapping operator. The first phase measurement $\varphi 1(x,y) \approx \varphi(x,y)$ is less than $1\lambda$ $(i.e.\ \varphi 1(x,y) \in (-\pi,\pi))$ otherwise this method does not work at all. The second phase $\varphi 2(x,y)$ is $G$-times more sensitive; meaning that $\varphi 2(x,y)$ is scaled-up by $G$ and therefore wrapped several times. The last step however is always to go from phase-radians to actual surface-height in centimeters or meters; this last step is shown in section 6 and it depends on the actual experimental set-up used to obtain the fringe patterns $I1(x,y)$ and $I2(x,y)$.

Let us now display our temporal 2-steps unwrapping formula as,

#234984 - $15.00 USD Received 24 Feb 2015; revised 24 May 2015; accepted 26 May 2015; published 8 Jun 2015

$$\varphi 2(x,y) = G\varphi 1(x,y) + W\left[\varphi 2_W(x,y) - G\varphi 1(x,y)\right], \text{ (radians).} \quad (6)$$

This is the main result of this paper and as far as we know this is a new and useful 2-sensitivity temporal phase-unwrapper. The estimated *unwrapped* phase $\varphi 2(x,y)$ is the searched continuous phase with the highest sensitivity. The term $G\varphi 1(x,y)$ is the first coarse estimation of $\varphi 2(x,y)$ and may be represented by,

$$G\varphi 1(x,y) = \varphi 2(x,y) + \varphi e(x,y). \quad (7a)$$

$$G\varphi 1(x,y) = 2\pi k(x,y) + \varphi 2_W(x,y) + \varphi e(x,y). \quad (7b)$$

The coarse estimate $G\varphi 1(x,y)$ equals $\varphi 2(x,y)$ plus an error phase $\varphi e(x,y)$ (Eq. (7a)). The integer 2D-field which unwraps $\varphi 2_W(x,y)$ is $k(x,y) \in \{\ldots,-2,-1,0,1,2,\ldots\}$. Substituting Eq. (7b) into Eq. (6) and rewriting Eq. (6) for the reader's convenience one obtains,

$$\begin{aligned}
\varphi 2(x,y) &= G\varphi 1(x,y) + W[\varphi 2_W(x,y) - G\varphi 1(x,y)], \\
\varphi 2(x,y) &= G\varphi 1(x,y) + W[\ \varphi 2_W(x,y) - 2\pi k(x,y) - \varphi 2_W(x,y) - \varphi e(x,y)], \\
\varphi 2(x,y) &= G\varphi 1(x,y) + W[-2\pi k(x,y) - \varphi e(x,y)].
\end{aligned} \quad (8)$$

Given that $\varphi e(x,y) = W[2\pi k(x,y) + \varphi e(x,y)]$ and using Eq. (7a) one obtains,

$$\begin{aligned}
\varphi 2(x,y) &= G\varphi 1(x,y) - \varphi e(x,y), \\
\varphi 2(x,y) &= \varphi 2(x,y) + \varphi e(x,y) - \varphi e(x,y), \\
\varphi 2(x,y) &= \varphi 2(x,y).
\end{aligned} \quad (9)$$

Equation (9) is valid whenever the phase *unwrapped* error $\varphi e(x,y) = [\varphi 2(x,y) - G\varphi 1(x,y)]$ do not exceed $1\lambda$, *i.e.* $\varphi e(x,y) \in (-\pi,\pi)$, that is,

$$\varphi e(x,y) = \left[\varphi 2(x,y) - G\varphi 1(x,y)\right] \in (-\pi,\pi). \quad (10)$$

We have mathematically demonstrated that our 2-sensitivity temporal phase-unwrapper obtains the unwrapped phase $\varphi 2(x,y)$ *completely untouched by the phase-error* $\varphi e(x,y)$ *of the first coarse phase estimate* $G\varphi 1(x,y) = \varphi 2(x,y) + \varphi e(x,y)$ whenever the condition in Eq. (10) is satisfied. Figure 1 shows graphically the difference between our 2-steps temporal phase unwrapper and the one reported in [3]. Note that if both $\varphi 1(x,y)$ and $\varphi 2_W(x,y)$ were noiseless and distortion-less $\varphi e(x,y) \approx 0$, the factor *G* could a large number.

In Fig. 1 we shows that in order to be at the Nyquist temporal sampling rate we need at least 9 phase-maps with phase sensitivities of $\{\lambda, 2\lambda, 3\lambda, \ldots, 9\lambda\}$ [3] to unwrap this sequence of 9 temporal phase-maps. In contrast using the 2-steps algorithm herein described, only the 2 extreme phase-maps $\{1\lambda, 9\lambda\}$ are needed.

#234984 - $15.00 USD Received 24 Feb 2015; revised 24 May 2015; accepted 26 May 2015; published 8 Jun 2015

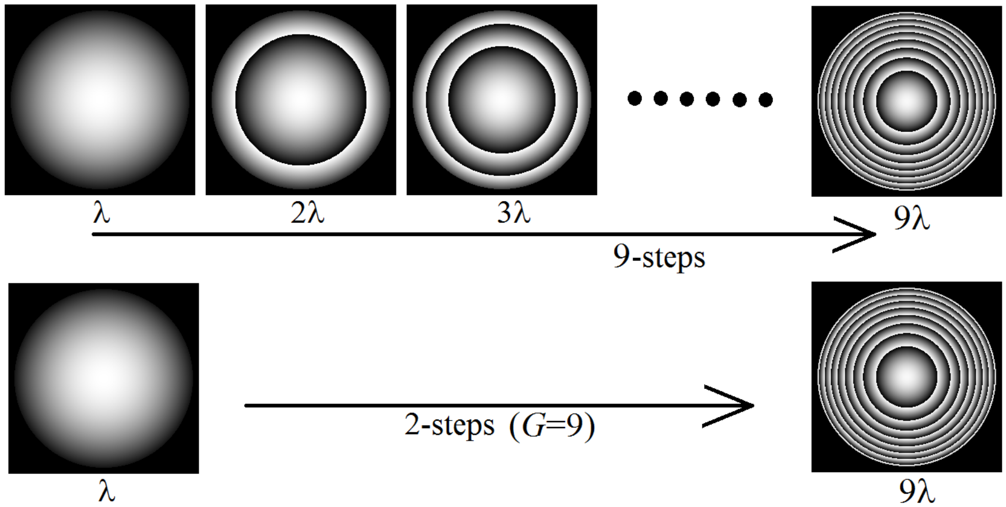


Fig. 1. At the top we show the 9 temporal samplings needed by standard temporal phase unwrapping [3] to pass from 1-lambda to 9-lambda in sensitivity at the Nyquist sampling rate. In our 2-step temporal phase unwrapper algorithm (Eq. (6) with $G = 9$) we only need the two extreme sensitive phase-maps to obtain the same results.

### 5. First computer simulation example with *G* = 10

As Fig. 2 shows an intrinsically discontinuous surface $\varphi 1(x,y)$ assumed to be 1-wavelenght ($1\lambda$) “height”, noisy and distorted.

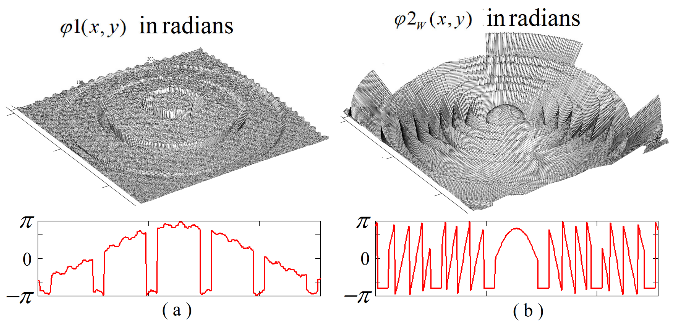


Fig. 2. Panel (a) shows the surfaces and central-cuts of the 1-wavelenght ($1\lambda$) phase $\varphi 1(x,y) \in (-\pi,\pi)$ containing 3-ring discontinuities. Panel (b) shows the *G*-times (*G*=10) more sensitivity wrapped phase $\varphi 2_W(x,y) = W[G\varphi(x,y)]$.

The second surface $\varphi 2_W(x,y)$ is wrapped and it is assumed to be noiseless and undistorted. This idealized condition is made to show that our first coarse estimation $G\varphi 1(x,y)$ errors do not propagate towards $\varphi 2(x,y)$. Figure 3 shows the unwrapping process where the rounded-plus-sign $\oplus$ represents our unwrapping algorithm (Eq. (6)). As Fig. 3 shows, the amplified phase $G\varphi 1(x,y) = 10\varphi 1(x,y)$ is noisy and distorted while $\varphi 2_W(x,y)$ and its unwrapped version $\varphi 2(x,y)$ have neither noise nor distortion.

#234984 - $15.00 USD Received 24 Feb 2015; revised 24 May 2015; accepted 26 May 2015; published 8 Jun 2015

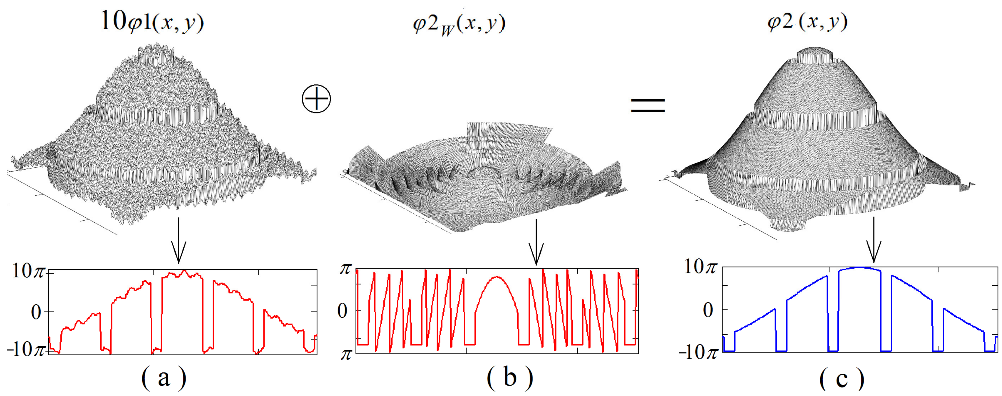


Fig. 3. Here we show the temporal unwrapping of a 3-rings discontinuous surface and their central-cuts; these 3 discontinuous rings are not wrapped-phase discontinuities, they are essential surface discontinuities. Panel (a) shows $G\varphi 1(x,y)=10\varphi 1(x,y)$. Panel (b) shows the noiseless wrapped-phase $\varphi 2_W(x,y)\in(-\pi,\pi)$. Panel (c) shows $\varphi 2(x,y)$ obtained using our 2-step temporal phase unwrapper.

Next Fig. 4 shows in gray levels, the phases corresponding to $10\varphi 1(x,y)$ and $\varphi 2(x,y)$. Observe the centered cut-lines in red for $G\varphi 1(x,y)$ and in blue for $\varphi 2(x,y)$. In panel (b) we have superimposed $G\varphi 1(x,y)$ and $\varphi 2(x,y)$ to have an intuitive estimation of the phase error $\varphi e(x,y)=\varphi 2(x,y)-10\varphi 1(x,y)$.

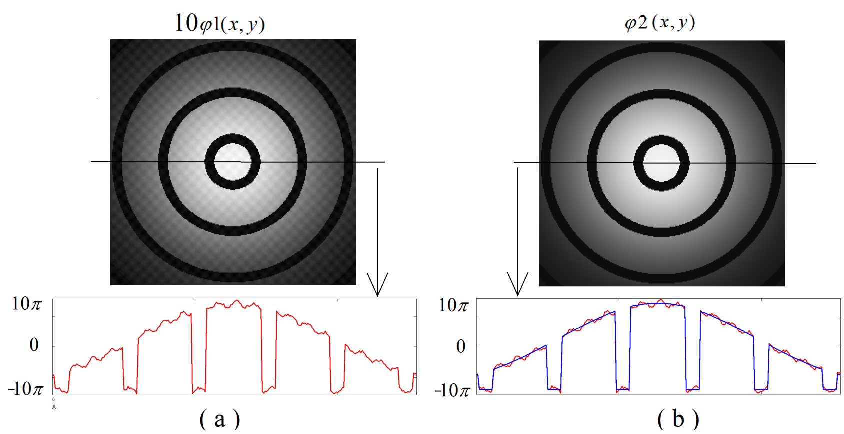


Fig. 4. Here we show the 3-rings discontinuous surface-phase in gray levels. Panel (a) shows the noisy and distorted 1-wavelenght phase $G\varphi 1(x,y)$ scaled-up by $G$=10. The red graph is a central cut of $10\varphi 1(x,y)$. Panel (b) shows in blue a cut-graph of the phase $\varphi 2(x,y)$. We have superimposed the red and blue graphs to see the error $\varphi e(x,y)$ between them.

Figure 5 shows that whenever $\left[\varphi 2(x,y)-10\varphi 1(x,y)\right]\in(-\pi,\pi)$ holds we end up with the desired high-sensitive unwrapped phase $\varphi 2(x,y)$ without the phase errors $\varphi e(x,y)$ generated by in our initial coarse approximation $10\varphi 1(x,y)=\varphi 2(x,y)+\varphi e(x,y)$.

#234984 - $15.00 USD Received 24 Feb 2015; revised 24 May 2015; accepted 26 May 2015; published 8 Jun 2015

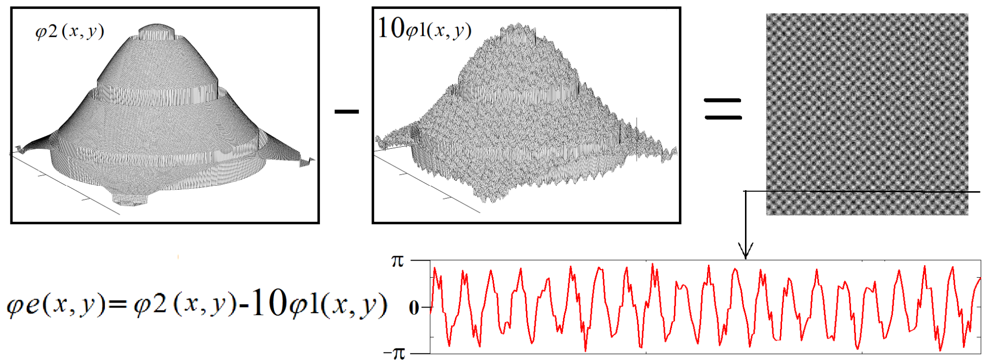


Fig. 5. This figure shows a crucial fact of the proposed phase unwrapping algorithm with $G$=10. The error between the more sensitive estimated *unwrapped* phase $\varphi 2(x,y)$ (in radians), and the scaled-up ($G$=10) phase $G\varphi 1(x,y)=10\varphi 1(x,y)$ must fall within $\varphi e(x,y)\in(-\pi,\pi)$.

Finally Fig. 6 shows what happens to the continuous (unwrapped) phase $\varphi 2(x,y)$ when the condition $[\varphi 2(x,y)-G\varphi 1(x,y)]\in(-\pi,\pi)$ do not hold; spurious phase jumps start to appear in $\varphi 2(x,y)$ (Fig. 6). This is a hallmark indication that we have exceeded the maximum allowed scaling-up $G$ factor. In this case we need to repeat the experiment with a lower $G$ and/or reduce the estimation error of $\varphi 1(x,y)$ until these spurious phase jumps disappear.

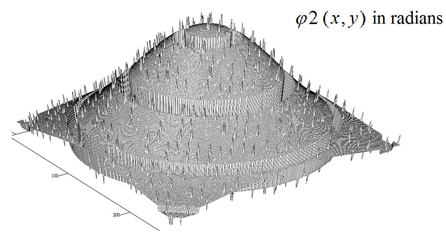


Fig. 6. Here have increased the sensitivity gain from $G$=10 to $G$=12 exceeding the boundaries of the condition $[\varphi 2(x,y)-G\varphi 1(x,y)]\in(-\pi,\pi)$, generating spurious phase jumps (in radians).

## 6. Second example: fringe-projection profilometry of a discontinuous surface

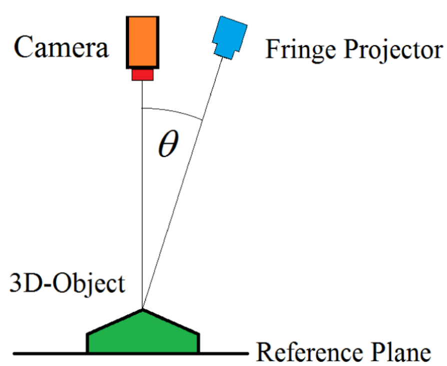


Fig. 7. This is the typical configuration to digitize a 3-dimensional (3D) object using fringe-projection profilometry. Theta is the angle between the camera and the fringe-projector.

#234984 - $15.00 USD Received 24 Feb 2015; revised 24 May 2015; accepted 26 May 2015; published 8 Jun 2015

Here we present a profilometry [15] example where the phase amplifying factor $G \in \mathbb{R}$ is set to seven ($G = 7$). The standard fringe-projection profilometry set-up is shown in Fig. 7.

In the absence of a 3D object, one obtains two pure carrier-fringe patterns projected over the reference plane,

$$\begin{aligned} I1(x,y)_{\text{Reference Plane}} &= a(x,y) + b(x,y)\cos[\ \ \omega_1 x + \varphi n(x,y)], \\ I2(x,y)_{\text{Reference Plane}} &= a(x,y) + b(x,y)\cos[7\omega_1 x + \varphi n(x,y)], \quad (G=7). \end{aligned} \tag{11}$$

From Eq. (11) the carrier-frequency in $I2(x,y)_{\text{Reference Plane}}$ is multiplied by $G = 7$ however the phase-noise $\varphi n(x,y)$ remains the same for both fringe patterns.

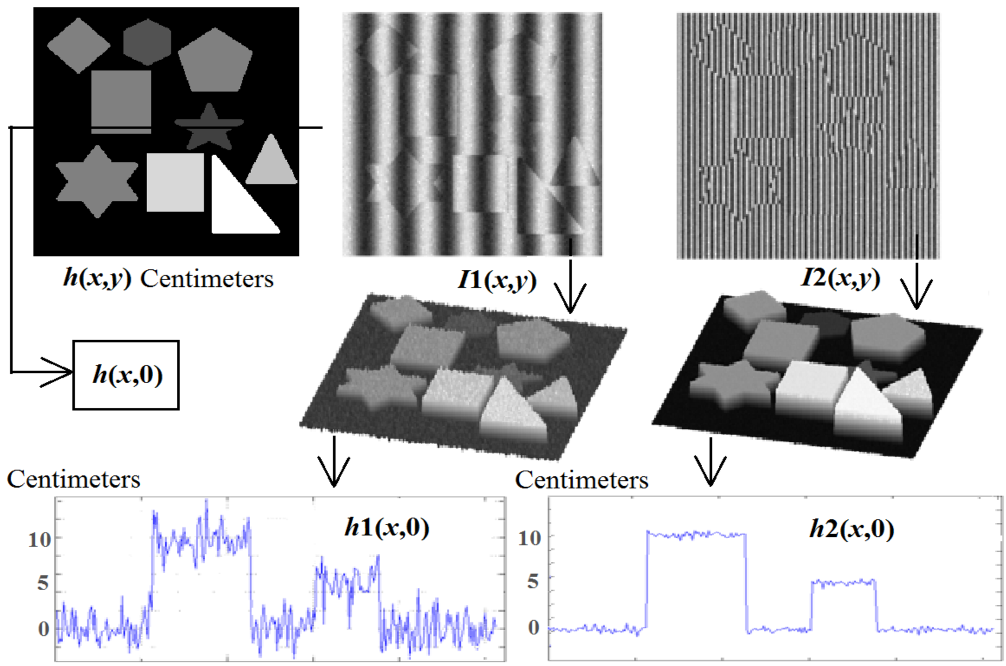


Fig. 8. Here a simulated fringe-projection profilometry experiment of a discontinuous surface containing 9 separated objects. The highest object is the whitest triangle. In the blue graphs we can see that the measuring noise in $h2(x,0)$ has decreased in amplitude 7-times with respect to $h1(x,0)$.

Figure 8 shows a computer simulated surface $h(x,y)$ having 9 objects with different heights coded in gray levels. These 9 objects are collocated over the reference plane. The two fringe patterns at the CCD camera sensor $I1(x,y)$ and $I2(x,y)$ are:

$$\begin{aligned} I1(x,y) &= a(x,y) + b(x,y)\cos[\ \ \omega_1 x + \ \ \omega_1 \tan(\theta) h(x,y) + \varphi n(x,y)], \\ I2(x,y) &= a(x,y) + b(x,y)\cos[7\omega_1 x + 7\omega_1 \tan(\theta) h(x,y) + \varphi n(x,y)]; \quad (G=7). \end{aligned} \tag{12}$$

The phase sensitivity of the fringe pattern $I1(x,y)$ is $\omega_1 \tan(\theta)$, while the phase sensitivity of $I2(x,y)$ is $7\omega_1 \tan(\theta)$. Phase-demodulating $I1(x,y)$ and $I2(x,y)$, and subtracting their carrier-frequency reference-planes $\omega_1 x$ and $7\omega_1 x$ one obtains,

#234984 - \$15.00 USD Received 24 Feb 2015; revised 24 May 2015; accepted 26 May 2015; published 8 Jun 2015

$$\begin{aligned}&\varphi 1(x,y)=\text{angle}\left\{\exp\left[i\,\omega_1\tan(\theta)h(x,y)+i\,\varphi n(x,y)\right]\right\};\,\varphi 1\in(-\pi,\pi),\\&\varphi 2_W(x,y)=\text{angle}\left\{\exp\left[i\,7\omega_1\tan(\theta)h(x,y)+i\,\varphi n(x,y)\right]\right\};\quad(G=7).\end{aligned}\tag{13}$$

The more sensitive wrapped phase $\varphi 2_W(x,y)$ is unwrapped according to Eq. (6) as,

$$\varphi 2(x,y)=7\,\varphi 1(x,y)+W\left[\varphi 2_W(x,y)-7\,\varphi 1(x,y)\right];\ \text{radians},\quad(G=7).\tag{14}$$

The last step is the physical calibration from radians to centimeters (cm) as,

$$h1(x,y)=\frac{\varphi 1(x,y)}{\omega_1\tan(\theta)}\ \text{cm};\qquad h2(x,y)=\frac{\varphi 2(x,y)}{7\,\omega_1\tan(\theta)}\ \text{cm}.\tag{15}$$

Substituting the demodulated phases $\varphi 1(x,y)$ and $\varphi 2(x,y)$ in Eq. (12) one obtains,

$$h1(x,y)=h(x,y)+\frac{\varphi n(x,y)}{\omega_1\tan(\theta)};\qquad h2(x,y)=h(x,y)+\frac{\varphi n(x,y)}{7\,\omega_1\tan(\theta)};\quad(G=7).\tag{16}$$

Equation (16) means that the height $h2(x,y)$ is 7-times *less-noisy* than $h1(x,y)$ (Fig. 8). Additionally, Eq. (16) is equivalent to Eq. (4), but now the height-noise reduction is expressed in terms of the noise-amplitude $\varphi n(x,y)$ not in terms of its power $\int|\varphi n(x,y)|^2\,dxdy$.

We finally emphasize that this profilometry simulated experiment would have required at least $N = 7$ phase-maps using standard temporal unwrapping [3]. However, using our 2-steps temporal unwrapping formula, one only needs the 2 extreme phase-maps (see Fig. 1) to achieve exactly the same results in terms of noise and harmonic distortion rejection.

## 7. Conclusions

We have presented a 2-steps temporal phase-unwrapping algorithm for measuring static surfaces. The first phase $\varphi 1(x,y)$ comes from a fringe-pattern phase-modulated by less than $1\lambda$. The wrapped phase $\varphi 2_W(x,y)$ is $G$-times more sensitive. This algorithm was demonstrated mathematically in section 4 and we repeated it here for the reader's convenience,

$$\varphi 2(x,y)=G\varphi 1(x,y)+W\left[\varphi 2_W(x,y)-G\varphi 1(x,y)\right],\quad(G\gg 1,\,G\in\mathbb{R}).\tag{17}$$

This unwrapping algorithm holds whenever,

$$\varphi e(x,y)=\varphi 2(x,y)-G\varphi 1(x,y)=W\left[\varphi 2_W(x,y)-G\varphi 1(x,y)\right].\tag{18}$$

If the above equality (Eq. (18)) is not fulfilled spurious phase jumps start to appear in the unwrapped phase $\varphi 2(x,y)$ (Fig. 6). In this case *we must repeat the experiment to decrease the amplifying sensitivity factor* $G\in\mathbb{R}$, *and/or decrease the phase-errors in* $\varphi 1(x,y)$. Just for completeness let us show the standard algorithm for temporal phase unwrapping [3,14] applied to $N\in\mathbb{Z}$ phase-maps $\{\varphi_W^0,\varphi_W^1,\ldots,\varphi_W^k,\ldots,\varphi_W^{N-1}\}$,

$$\varphi^{k+1}(x,y)=\varphi^k(x,y)+W\left[\varphi^{k+1}(x,y)-\varphi_W^k(x,y)\right];\ \sup\left|\varphi_W^0(x,y)\right|<\lambda.\tag{19}$$

This unwrapping algorithm is valid whenever the Nyquist temporal sampling rate is observed,

$$\sup\left|\varphi^{k+1}(x,y)-\varphi^k(x,y)\right|<\lambda,\quad k=\{0,1,\ldots,N-1\}.\tag{20}$$

#234984 - $15.00 USD Received 24 Feb 2015; revised 24 May 2015; accepted 26 May 2015; published 8 Jun 2015

We finally list the advantages and limitations of our new 2-steps (2-sensitivities) temporal phase unwrapping algorithm to measure static surfaces with high precision, and compare it against the *N*-steps standard (Eq. (19) and Eq. (20)) temporal phase unwrapper [3].

a) One needs 2-sensitivity fringe-patterns phase-modulated fringe-patterns. One modulated by $\varphi(x,y) \in (-\pi,\pi)$ and another one by $G\varphi(x,y)$ ($G >> 1.0, G \in \mathbb{R}$) of the static surface under test. The amplifying *G* parameter in practice typically falls within $(8 < G < 14)$ (see Fig. 1).

b) The demodulated phase $\varphi 1(x,y) \approx \varphi(x,y)$ must be less than $1\lambda$ sensitivity.

c) The wrapped phase $\varphi 2_W(x,y)$ is *G*-times more sensitive than $\varphi 1(x,y)$.

d) The unwrapped phase $\varphi 2(x,y)$ is roughly approximated by $\varphi 2(x,y) \approx G\varphi 1(x,y)$

e) Substituting $G\varphi 1(x,y)$ and the wrapped phase $\varphi 2_W(x,y)$ into our 2-step phase unwrapping algorithm (Eq. (6) or Eq. (17)) one obtains the desired unwrapped phase $\varphi 2(x,y)$ without the errors contained in the first estimation of $\varphi 1(x,y)$.

f) If the phase error $\varphi e(x,y)$ (Eq. (10)) lies outside $(-\pi,\pi)$ spurious phase jumps start to appear. Then we need to repeat the experiment with a lower *G*, and/or obtain a less noisy and/or less distorted $1\lambda$ estimation of $\varphi 1(x,y)$.

g) If (for example) we increase the phase sensitivity from $1\lambda$ to $9\lambda$, both the standard temporal phase unwrapper [3] and our 2-steps one, would give the same unwrapping results. But the standard temporal unwrapper [3] would require at least 9 phase-maps while our 2-step unwrapper requires only the 2 extreme phase-maps (see Fig. 1).

h) The same applies to the demodulated phase-noise $\varphi n(x,y)$. For example a 7-step (with $1\lambda$ sensitivity increase) using the standard unwrapper [3] would increase 49-times the signal-to-noise power ratio (see Eq. (4)) with reference to the estimate $\varphi 1(x,y)$. This is the same amount of signal-to-noise increase obtained using our 2-step temporal unwrapper using only the $1\lambda$ and $7\lambda$ phase-maps sensitivities (see Fig. 8).

In brief, all anti-noise benefits of *N*-steps $\{\varphi_W^0, \varphi_W^1, \ldots, \varphi_W^{N-1}\}$ standard temporal phase unwrapping [3] (Eqs. (19) y (20)) are kept unchanged, except that we are using only the 2 extreme phase-maps $\{\varphi^0, \varphi_W^{N-1}\}$ (see Fig. 1 and Eq. (6)); this holds whenever the condition in Eq. (10) is maintained.

**Acknowledgments**

We would like to acknowledge the support of the Mexican Scientific Research Council (CONACyT) for his valuable support through the basic research grant 157044-F.